Electronic Raman Studies of Antiferromagnetic Dysprosium Aluminum Garnet below T_N and with and without an Applied Magnetic Field*

B. E. Argyle,† Joan L. Lewis, R. L. Wadsack, ‡ and R. K. Chang
Becton Center, Yale University, New Haven, Connecticut 06520
(Received 25 February 1971)

Electronic Raman transitions within the $^6H_{15/2}$ and to the $^6H_{13/2}$ manifolds of antiferromagnetic dysprosium aluminum garnet (DyAlG) at 1.5 K ($T_N = 2.5$ K) have been observed. Comparison of the Raman spectra obtained when a magnetic field (18 kOe) was applied along the [001] direction and when $H_{app} = 0$ yielded estimations for the following: (a) the internal field splittings and consequently the exchange fields of the first two excited Kramers doublets in $^6H_{15/2}$; and (b) the Zeeman splittings of these levels. Using wave functions from our crystal-field analysis (Wadsack *et al.*), the g values of all the levels in the $^6H_{15/2}$ and $^6H_{13/2}$ manifolds have been calculated. These compared well with the g values previously observed (Aoyagi *et al.*) and with our Raman determination of $g_z = 14.7 \pm 1$ for the lowest level in $^6H_{13/2}$. Contributions to the electronic Raman scattering tensors from the six magnetic sublattices were derived for the applied field along [001] and for the different combinations of incident and scattered polarizations. Using the crystal-field wave functions for DyAlG, the relative Raman intensities for the observed Raman transitions were calculated. These Raman intensities are as sensitive to the crystal-field wave functions as are the g values. The calculated and observed Raman intensity ratios for various polarization combinations agreed only qualitatively. Breakdown of phonon polarization selection rules for the E_g and A_{1g}, but not the T_{2g} Raman-active phonons, was observed when $H_{app} = 18$ kOe. No explanation was given for this observation.

I. INTRODUCTION

Recently the optical-absorption and fluorescence spectra of antiferromagnetic dysprosium aluminum garnet (DyAlG) at temperatures below its Néel temperature ($T_N = 2.5$ K) have been extensively studied[1-5] in order to understand the interactions among neighboring Dy^{3+} ions. Previous work on the magnetic and thermal properties of DyAlG has been discussed at length in a recent paper by Landau *et al.*[6] Suffice it to mention that in spite of the structural complexity of DyAlG (O_h^{10} space group), its magnetic properties for $T < T_N$ can be described simply by an Ising model. This is because the crystal field of DyAlG produces a highly anisotropic g value for the ground state ($g_z = 18.1$, $g_y \approx 0.4$, $g_x \approx 0.7$).[7]

Below T_N the magnetically anisotropic Dy^{3+} ions order antiferromagnetically into six magnetic sublattices with their moments pointed either parallel or antiparallel to one of the three principal axes (X, Y, Z) of the cubic unit cell. Such a configuration of antiferromagnetically aligned spins has been labeled as (A_1, A_1, A_1) by Wolf *et al.*,[8] where A_1 represents antiferromagnetic alignment and the order within the brackets is (X, Y, Z). In this (A_1, A_1, A_1) configuration, the Kramers degeneracy of each of the crystal-field levels is split primarily by the long-range magnetic dipole-dipole interaction and by the short-range exchange interaction. The dipolar contribution to the internal field at the ith site is given by

$$\sum_j \left(\frac{3\vec{\mu}_j \cdot \vec{r}_{ij}}{|r_{ij}|^5} \vec{r}_{ij} - \frac{1}{|r_{ij}|^3} \vec{\mu}_j \right) \tag{1}$$

and is independent of the electronic state of the ith ion. The contrary is true for the exchange contributions to the internal field, where both the isotropic and anisotropic exchange may become important.[9,10]

At 1.5 K, upon the application of a large magnetic field ($H_{app} > 6$ kOe) parallel to [001], the spins aligned along $-Z$ will be flipped to the $+Z$ direction. The spins which were formerly antiferromagnetically aligned along X and Y will be disordered. Such a spin configuration has been designated as (P_d, P_d, P_m) where P denotes paramagnetism within the spin structures and the subscripts d and m denote a disordered and magnetized state, respectively.[8] The contributions of the dipolar and exchange fields in the (P_d, P_d, P_m) configuration are different from those of the ordered (A_1, A_1, A_1) configuration. One of the purposes of this paper is to measure such differences by Raman scattering.

Recently, we have reported the light scattering by the Raman-active phonons ($3A_{1g}$, $8E_g$, $14T_{2g}$) and by the electronic levels of Dy^{3+} in DyAlG and in DyGaG cooled to 80 K.[11] In that paper (hereafter referred to as Paper I), the Raman determinations for the $^6H_{13/2}$ and $^6H_{15/2}$ manifolds were used to supplement the absorption data of Grünberg *et al.*[12]

for the other higher manifolds in order to carry out a complete crystal-field (CF) analysis appropriate for the D_2 local symmetry of the Dy^{3+} site.

The CF wave functions obtained in Paper I were used in this paper to calculate the g-tensor components $(g_z, g_{x,y})$ for all levels in the $^6H_{13/2}$ and $^6H_{15/2}$ manifolds. Using both these calculated g values and the observed shifts and splittings of Raman spectra in DyAlG at 1.5 K with and without a magnetic field along [001], we are able to estimate the magnetic interaction fields in the (A_1, A_1, A_1) and (P_d, P_d, P_m) configurations for several electronic levels in the $^6H_{13/2}$ manifolds. In addition, the CF wave functions obtained in Paper I were also used in this work to calculate separately the relative Raman intensity due to transitions in those Dy^{3+} ions aligned parallel to and those aligned transverse to the applied field direction. Such intensity calculations were found helpful in assigning the peaks in the observed Raman spectra to specific electronic transitions.

The experimental methods are described in Sec. II. Results pertaining to the $^6H_{15/2}$ and the $^6H_{13/2}$ manifolds are discussed, respectively, in Secs. III and IV. In Sec. V, relative Raman intensities are presented. Some unexpected peculiarities observed in the scattering intensity of several Raman-active phonons in the presence of an applied magnetic field are presented in Sec. VI. The conclusions are summarized in Sec. VII.

II. EXPERIMENTAL DETAILS

Our Raman scattering apparatus and geometry are by now conventional. An argon laser provided the exciting radiation at 5145 Å with 300 mW, and the 90° scattered Raman radiation was collected through appropriate lenses and focused on a Spex model-1400 double monochromator having two 600-g/mm gratings blazed for 1.25 μ. All data were recorded at second order which enhanced our spectral resolution. The weak Raman signal was detected by a magnetically defocused and cooled EMI 9558A photomuliplier. Its signal, consisting of current pulses, was amplified by a preamp, processed by a discriminator (LeCroy No. 133A), and counted by a ratemeter (Hammer No. N-751).

The DyAlG single crystal (flux-grown) was immersed in a narrow tip (o.d. = 16 mm) liquid-helium Dewar which was pumped continuously (Welch vacuum pump No. 1397). The temperature of the helium coolant (1.5 K) was determined by monitoring its vapor pressure with a Wallace and Tiernan pressure indicator. This temperature could be held constant to ±0.02 K for over 10 h with the intense laser beam focused within the DyAlG.

A 4-in. electromagnet with 1-in. tapered Fe-Co pole pieces separated by 0.71 in. provided the applied magnetic field. The magnetic field strength was measured by a Hall probe gaussmeter.

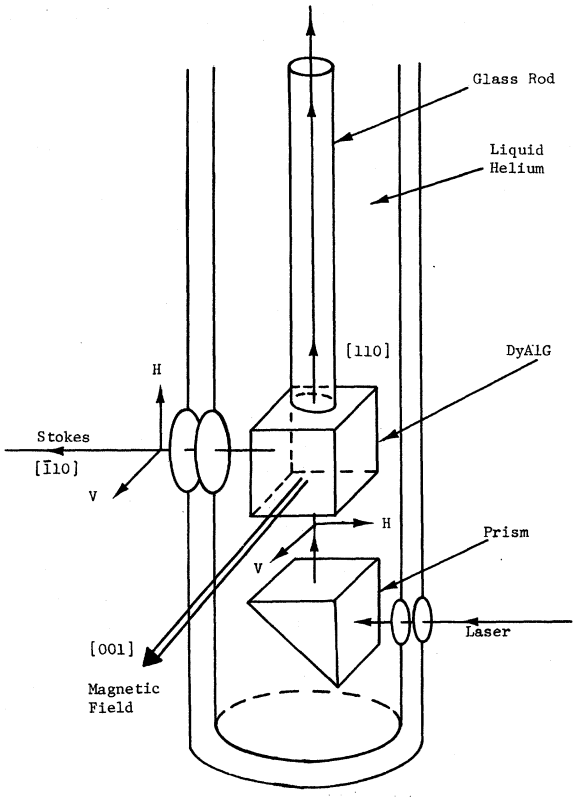

FIG. 1. Experimental diagram specifying the orientation of the DyAlG crystal with respect to the magnetic field direction, and the directions of propagation and polarization of the incident laser and scattered Stokes radiations. The polarization notation (*H-H*, *H-V*, *V-V*, *V-H*) used throughout the text refers to this orientation for the incident-scattered polarizations. The glass rod, the DyAlG, and the right-angle prism were held rigidly together by a brass sleeve. The whole assembly was immersed in the liquid-helium Dewar.

The orientation of the DyAlG crystal ($2.5 \times 2.8 \times 3.6$ mm^3) with respect to the incident and scattered light propagation direction and its polarization vector is shown in Fig. 1. This orientation was shown previously in Paper I to be an optimum orientation for both isolating frequencies and determining symmetries, i.e., A_{1g}, E_g, or T_{2g}, of Raman-active phonons. In the present experiment, the strict adherence to the phonon selection rules was used to ascertain our crystal orientation (within 5°).

The DyAlG crystal and an attached right-angle glass prism were mounted onto a fused-quartz light-pipe rod (Fig. 1). This assembly was prealigned (within 3°) during assembly using a microscope, glued together, and installed in the helium

Dewar. The light-pipe rod was held by an O-ring vacuum seal and emerged through the top of the Dewar. A polished end face of the rod then allowed this arrangement to provide the most efficient removal of laser energy from the cryogenic environment. By viewing the pattern of transmitted laser radiation, the final rotational alignment of the crystal *in situ* could be made to within ~ 3° with respect to the incident laser beam. That is, the proper alignment could be "tuned in" by rotating the light-pipe rod until the transmitted radiation had a circular pattern of minimum size. Positioning the right-angle prism inside the Dewar, rather than outside and below, also avoided absorption and/or scattering of the laser beam from particles of frozen water vapor or air which might settle to the Dewar bottom.

III. $^6H_{15/2}$ MANIFOLD

As a prelude to interpreting our Raman scattering results, we review what is already known about the electronic ground state. It is now well established that for $T < T_N$ and $H_{app} = 0$, the ground-state doublet of DyAlG ($g_z = 18.2$, $g_{x,y} \approx 0$)[13] is split (see Table I) by both the dipole-dipole field expressed in Eq. (1) and by the exchange field. A dipolar lattice sum has been calculated for this (A_1, A_1, A_1) spin configuration by Gehring *et al.*[4] and by Ball *et al.*[14] The best value of the dipolar field was $H_d = 4.65$ kOe, of which 3.4 kOe was due to the four nearest neighbors. However, in order to explain the experimental data for the ground-state splitting, numerous workers have found it necessary to include additional nearest-neighbor interactions (called exchange interactions for convenience). This exchange field was reported[15,16] to be 52% of the nearest-neighbor dipolar field, or 1.77 kOe. As was stated in Sec. I, the dipolar field at site i is independent of the electronic state of ion i, while the exchange field, being related to overlap of wave functions, is definitely dependent on the state of ion i.

TABLE I. Summary of published data on the ground-state splitting due to dipolar and exchange interactions in DyAlG for $T < T_N$.

$\Delta(0)$ (cm^{-1})	
5.2 ± 0.5 [a]	optical
5.3 ± 0.10 [b,c]	optical
5.27 ± 0.10 [d]	optical
5.28 ± 0.05 [e]	magnetocaloric

[a] Hüfner *et al.*, Physik Kondensierten Materie 4, 108 (1965).
[b] Reference 4.
[c] Reference 2.
[d] Reference 5.
[e] Reference 8.

At $T = 1.5$ K and $H_{app} > 5$ kOe applied along [001], DyAlG is in the magnetized phase exhibiting the (P_d, P_d, P_m) spin configuration. The dipolar field and the exchange field acting on the ground-state ion are now reduced to less than 0.5 kOe.[17] Since these fields are small compared to an applied field of 18 kOe, we shall henceforth neglect their contribution in our future calculations involving the ground-state Zeeman splitting in the (P_d, P_d, P_m) configuration.

The g-tensor components for the ground state and the first two excited states of the $^6H_{15/2}$ manifold have been experimentally determined by several workers. Their results are summarized in Table II. Using the wave functions from our CF analysis reported in Paper I, the g values for all the CF levels in the $^6H_{15/2}$ and $^6H_{13/2}$ manifolds are also summarized in Table II. The agreement between calculated and experimental g values is good. It should be noted that only the ground state and the lowest two levels of $^6H_{13/2}$ are highly anisotropic and therefore are able to be approximated by an Ising model of the form

$$H_m = \sum_{i>j} K_{ij} S_i^z S_j^z .$$

A. 0-1 Transition

Figure 2 shows the Raman spectra for the electronic Raman transition from the ground state 0 to the first excited state 1.

With $H_{app} = 0$ kOe, a single peak (I) at 72.2 cm^{-1} was observed. At 18 kOe along [001], two peaks (II and III) were observed at 70.2 and 74.2 cm^{-1}, respectively. These observations can be explained simply with the aid of the level diagram in Fig. 3. Peak I involves a transition in the (A_1, A_1, A_1) configuration from the lower level of the ground state to the lower level of the excited state. The transition to the upper level of the excited state is predicted to be small by the ΔJ_z selection rules.

Peak II involves transitions in the disordered transverse ions (see Fig. 3) from the approximately degenerate ground states (nearly equally populated at 1.5 K owing to $g_{x,y} < 1$) to the weakly Zeeman split excited states (split according to $g_{x,y} = 4.5$, 3.7). Consequently, the centroid of these transitions $(70.2\ cm^{-1})_{av}$ should equal in wave number the 0-1 transition measured at $T > T_N$. Grünberg *et al.*,[12] Aoyagi *et al.*,[3] Gehring *et al.*,[4] Mace *et al.*,[18] and Wadsack *et al.*[11] reported the latter to be 70, 70.3, 70.1, 71, and 69 cm^{-1}, respectively. The broad width associated with peak II of Fig. 2 would be expected from a double transition from an almost degenerate ground state to a slightly split excited state (not resolvable, note slitwidth in Fig. 2).

The significant information contained in Fig. 2 is the wave-number difference between peak II

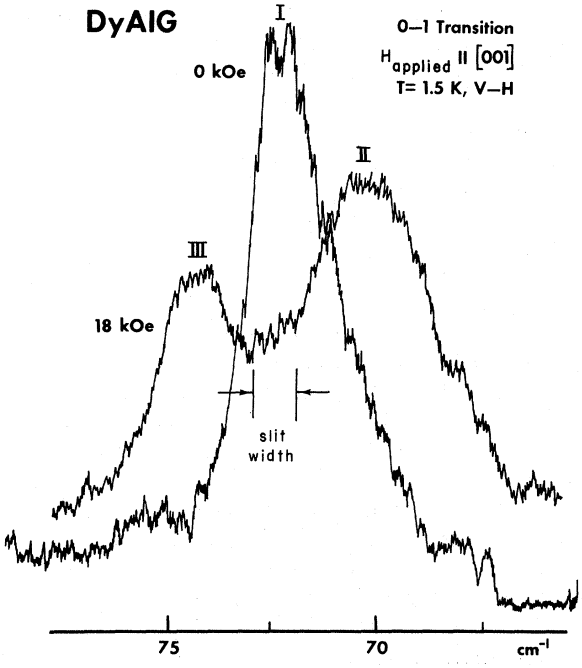

FIG. 2. Raman spectra of DyAlG at 1.5 K involving electronic transitions from the ground state 0 to the first excited state 1 of the $^6H_{15/2}$ manifold. Peak I was observed with $H_{app}=0$ kOe, while peaks II and III were observed with $H_{app}=18$ kOe along [001]. The incident and scattered polarizations were *V-H* (see Fig. 1).

and peak I (2.0 cm^{-1}). Since peak II effectively involves electronic transitions between levels which are only weakly perturbed by the external and internal fields, the relative shift of peak I must be due to the effect of the internal field (recall $H_{app}=0$) associated with the (A_1, A_1, A_1) configuration. Since we know the (A_1, A_1, A_1) ground-state splitting to be $\Delta(0)=5.3$ cm^{-1},[4,5,8] the splitting of the level 1 must be $\Delta^*(0)=1.3$ cm^{-1}. We can now solve for the exchange field in this level, $H^*_{ex}(0)$, if we use $g_z=12.5$[3] and use the known dipolar field $H_{dip}(0)=4.65$ kOe[4] (same as in the ground state). The exchange field of the first excited state in the (A_1, A_1, A_1) configuration is $H^*_{ex}(0) = -2.4$ kOe. This is remarkably different from that for the ground state, $H_{ex}(0)=+1.77$ kOe.

The wave-number difference between the Zeeman split peaks II and III contains information of the exchange field $H^*_{ex}(18)$ on level 1 in the ions with the z spins aligned along $+Z$ (see Figs. 2 and 3). The ground states of the Z-directed spins (parallel) are Zeeman split by

$$\Delta_{Zeeman}(18)=g\mu_B(H_{app}-NM) = 18.4(18-1.6)/21.4=14.1\ cm^{-1}, \quad (2)$$

where $N=\frac{4}{3}\pi$ (assuming the demagnetization factor of a sphere) and $M\approx 0.4$ kOe.[19] Both the dipolar and exchange field are negligible for the ground-

TABLE II. Calculated g values for the electronic states in the $^6H_{15/2}$ and $^6H_{13/2}$ manifolds. Published experimental g values are listed for comparison purposes.

			Calculated[a]		Experimental		
	Assign.	Raman[b] 80 K (cm^{-1})	$\lvert g_z\rvert$	$\lvert g_{x,y}\rvert$	$\lvert g_z\rvert$	$\lvert g_{x,y}\rvert$	
$^6H_{13/2}$	6′	3968	0.1	16.2, 0.3			
	5′	3832	3.7	0.6, 12.1			
	4′	3786	1.9	6.1, 6.0			
	3′	3719	0.1	7.6, 7.6			
	2′	3673	1.8	5.7, 10.7			
	1′	3594	13.4	0.2, 0.1			
	0′	3565	15.0	0.2, 0.1	14.7±1.0		Raman[a]
$^6H_{15/2}$	7		≈0	19.7, ≈0			
	6		11.0	0.5, 8.8			
	5		10.4	0.5, 8.5			
	4		0.9	13.7, 1.6			
	3	186	6.8	3.4, 8.6			
	2	114	10.4	4.1, 2.5	10.5		optical[c]
	1	69	11.1	4.5, 3.7	12.5		optical[c]
	0	0	17.8	0.8, 0.5	18.7		optical[c]
					18.4±0.5	0.5±0.2	optical[d]
					18.2	≈0	[e]

[a]This work.
[b]Reference 11.
[c]Reference 3.
[d]Reference 5.
[e]Reference 13.

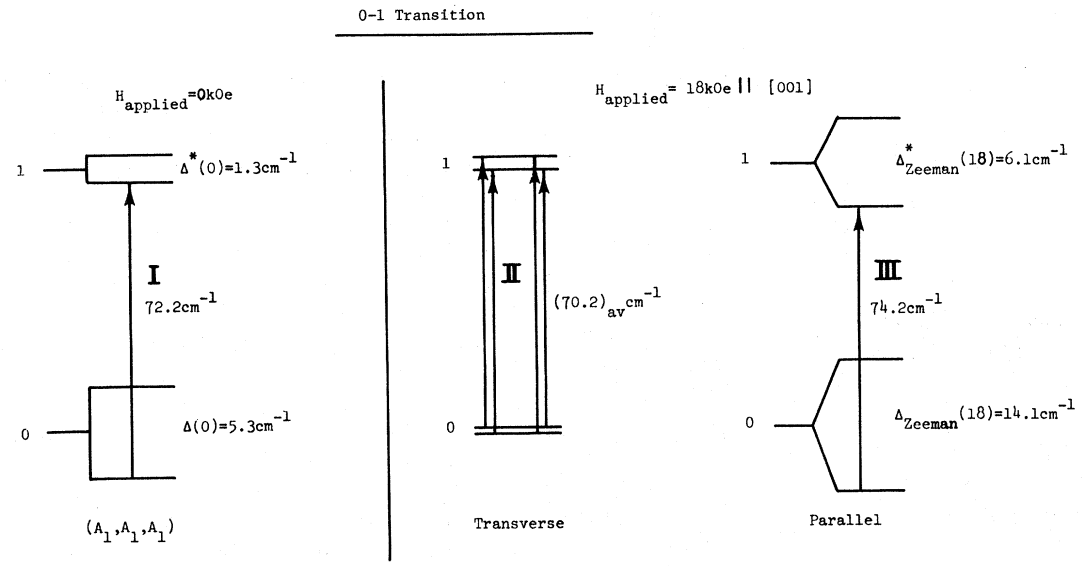

FIG. 3. Summary and assignment of the electronic Raman spectra shown in Fig. 2 which involved 0-1 transitions. Peaks I, II, and III involve transitions among electronic levels with the spins in the (A_1, A_1, A_1), transverse to H_{app} (P_d, P_d, P_m), and parallel to H_{app} (P_d, P_d, P_m), respectively. (See Sec. III A.)

state (P_d, P_d, P_m) configuration.

The Zeeman splitting for the Z-oriented spins in level 1 is

$$\Delta^*_{\text{Zeeman}}(18) = g^*\mu_B[H_{app} - NM + H^*_{ex}(18)]$$
$$= 12.5[16.4 + H^*_{ex}(18)]/21.4 . \quad (3)$$

The 4-cm^{-1} separation of peaks II and III therefore requires $\Delta^*_{\text{Zeeman}}(18) = 6.1$ cm^{-1}. The exchange field for the Z-oriented spins in level 1 with (P_d, P_d, P_m) configuration is $H^*_{ex}(18) = -6$ kOe. Note that this has the same sign as $H^*_{ex}(0) = -2.4$ kOe. That is, the exchange field for level 1 was found to be negative for both (A_1, A_1, A_1) and for the Z-directed spins of (P_d, P_d, P_m). The fact of their different strengths implies the presence of anisotropic exchange.[10]

We have measured the shift of peak III from peak II at several H_{app} (all greater than 5 kOe) and found the high-field slope to give a g_z consistent with $g_z = 12.5$ observed by Aoyagi *et al.*[3]

B. 0-2 Transition

The Raman spectra observed without and with an applied field (18 kOe) along [001] were similar to those observed for the 0-1 transition. The results are summarized in Fig. 4. Peak I, measured with $H_{app} = 0$, occurred at 118 cm^{-1} and corresponds to the transition from the lower level of the ground state 0 to the upper level of the excited state 2. A weaker peak was simultaneously observed at 111 cm^{-1} (peak I′), corresponding to the transition to the lower level of the excited state. Peaks I and I′ require $\Delta^*(0) = 7$ cm^{-1}.

With $H_{app} = 18$ kOe along [001], a broad peak at 112 cm^{-1} (peak II) and at 124 cm^{-1} (peak III) were observed. As stated before, the wave-number difference between peaks I and II determines the excited-state splitting $\Delta^*(0)$ caused by the internal fields when the spin configurations are (A_1, A_1, A_1). This gives $\Delta^*(0) = 6.7$ cm^{-1}, which is consistent with the 7-cm^{-1} splitting we deduced from peaks I and I′ (see Fig. 4). Using $g^*_z = 10.5$[3] (see Table II) and $H_{dip}(0) = 4.65$ kOe[4] (H_{dip} does not depend on the state of the ion), the exchange field acting on the excited state 2 in the (A_1, A_1, A_1) configuration is $H^*_{ex}(0) = 9$ kOe.

The wave-number difference between peaks II and III is 12 cm^{-1} (see Fig. 4). Since the Zeeman splitting of the ground state is 14.1 cm^{-1} [Eq. (2)], the Zeeman splitting of the excited state 2 [Eq. (3) with $g^*_z = 10.5$] must be $\Delta^*_{\text{Zeeman}}(18) = 9.9$ cm^{-1}. Hence, in the (P_d, P_d, P_m) configuration, the Z-oriented spins (parallel) in the excited state 2 must experience an exchange field of $H^*_{ex}(18) = 3.8$ kOe. This again has the same sign as $H^*_{ex}(0) = 9$ kOe.

In summary, the electronic Raman spectra pertaining to the $^6H_{15/2}$ manifold measured at $T = 1.5$ K with $H_{app} = 0$ and $H_{app} = 18$ kOe along [001] enabled us to deduce for the excited states 1 and 2 the exchange field $H^*_{ex}(0)$ in the (A_1, A_1, A_1) configuration, and the exchange field $H^*_{ex}(18)$ for the Z-oriented spins in the (P_d, P_d, P_m) configuration. To our knowledge, these exchange fields have never been reported previously.

The choice of applying the magnetic field along

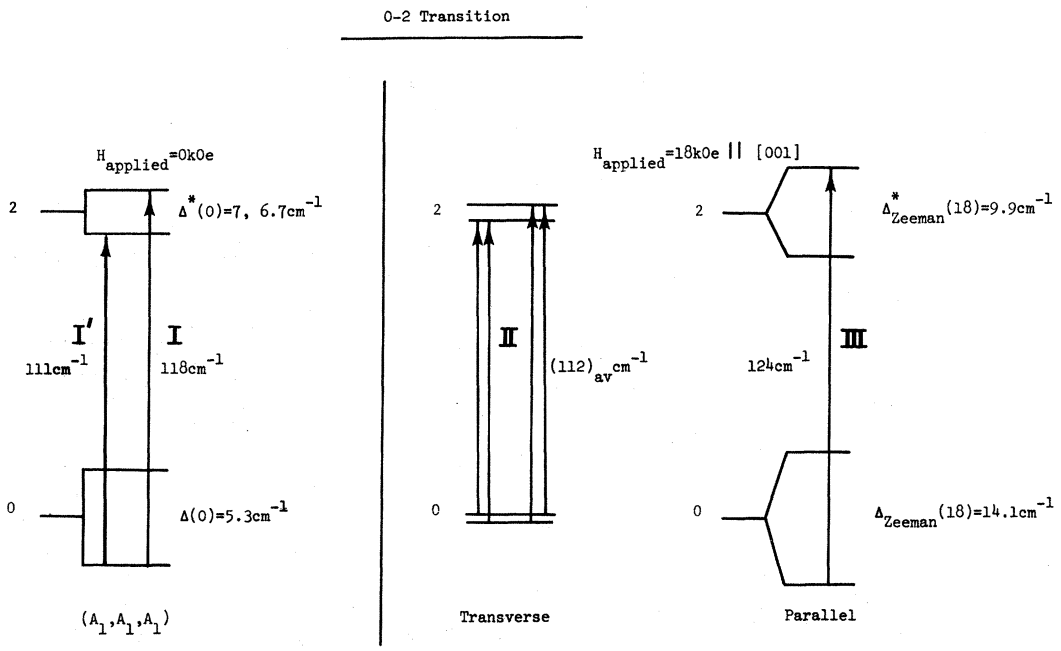

FIG. 4. Summary and assignment of the observed electronic Raman spectra involving 0-2 transitions. Peaks I and I′ were observed for the (A_1, A_1, A_1) spin configurations. Peaks II and III pertain to spins in the (P_d, P_d, P_m) configuration oriented transverse and parallel, respectively, to the H_{app} direction [001]. (See Sec. III B.)

[001] enabled us to use transitions associated with the transverse spins (P_d) with small $g_{x,y}$ as a reference wave-number marker. Its wave number is equal to the energy that the excited state would have at $T = 1.5$ K, if the applied dipolar and exchange fields were all zero. Consequently, its wave number is equal to the energy difference of the centroids of the excited-state doublet and the ground-state doublet. The shift due to the Zeeman splittings of the levels in the ions with the Z-oriented spins can thus be accurately measured as the shift from that reference wave-number marker. Had we applied the field along [111], the spin configuration would have been $[P_m, P_m, P_m]$[8]; that is, all the Dy^{3+} sites would be magnetically equivalent and magnetized paramagnetically along $+X$, $+Y$, and $+Z$ directions. In spite of its simplicity compared to the $[P_d, P_d, P_m]$ configuration used in this experiment, we would then have had no means of measuring the excited-state energies at 1.5 K in the presence of no applied and internal fields. These excited-state energies at 1.5 K could have been inferred from those measured at $T > T_N$, where the short-range order becomes negligible.[13] However, such inference would have required the assumption that the crystal-field separation at, for example, 20 K would be the same as at 1.5 K, where all the rest of the Zeeman and internal field Raman measurements were observed. The mixed phase of Dy^{3+} spins (P_d, P_d, P_m) which results from applying $\vec{H}_{app}$ along [001] thus adds to the accuracy of this experiment in determining $H^*_{ex}(18)$ (involves difference between peaks II and III).

The determination of $H^*(0)$ is less accurate because peaks I and II are on separate sweeps of the spectrometer. We improve on this by taking several measurements repeated in succession. We found the deviation to be ± 0.4 cm^{-1}.

IV. $^6H_{13/2}$ MANIFOLD

The analysis used in Sec. III for the 0-1 and 0-2 transitions could be applied again to the observed electronic Raman spectra for electronic transitions from the ground state to the lowest level, 0′, of the $^6H_{13/2}$ manifold. Within our experimental error, we did not observe (see Fig. 5) any shift between peak I ($H_{app} = 0$) and peak II ($H_{app} = 18$ kOe). This means that the interaction splittings of the two levels 0 and 0′ in the (A_1, A_1, A_1) configuration were equal to within our experimental accuracy. The wave number of peak II remained field independent, as expected from the small values of $g_{x,y}$ for both the ground state 0 and the excited state 0′ (see Table II). The shift of peak III with respect to peak II as a function of the applied field determines a g_z value for this excited state. We experimentally found $g_z = 14.7 \pm 1.0$, which is in excellent agreement with our calculated value of $g_z = 15.0$. To our knowledge the g values

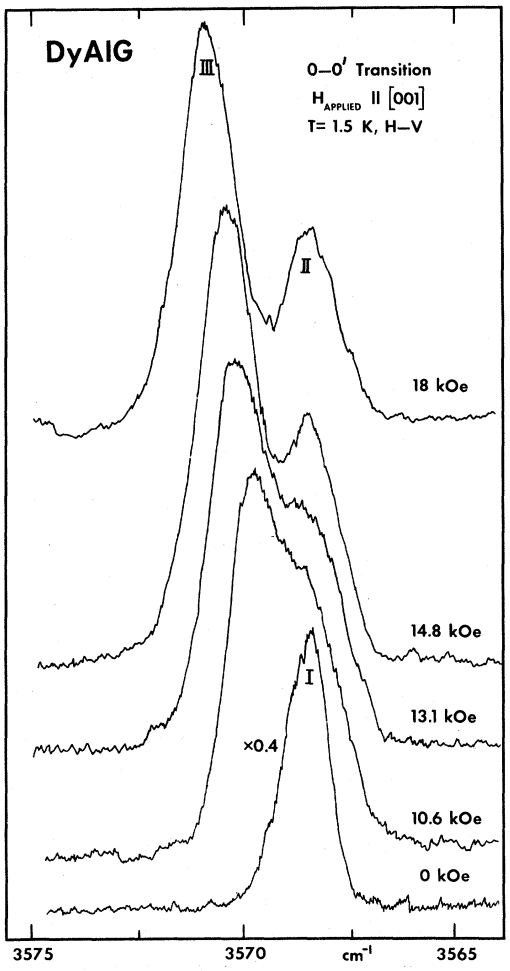

FIG. 5. Raman spectra of DyAlG at 1.5 K involving electronic transitions from the ground state 0 to the lowest level 0′ of the $^6H_{13/2}$ manifold. Peak I was observed with $H_{app}=0$ kOe, while peaks II and III were observed with different magnetic field strengths shown in the figure. As peak II involves transverse oriented spins, its position remained independent of field. The position of peak III, which involves parallel oriented spins, varied linearly with the magnetic field strength. The polarization combination was H-V.

of the $^6H_{13/2}$ manifold have never been reported in DyAlG. In the dilute garnet YAlG:Dy, $g_z=14.3$ and $g_{x,y}=1.1$ have been reported[12] for the lowest level we call 0′ in $^6H_{13/2}$.

V. RELATIVE INTENSITIES

The calculation of relative Raman intensities in garnets has been discussed in Paper I. In that paper, since the energy level structure of each ion was the same, we decomposed the incident and scattered polarization vectors along each of the Dy^{3+} sites, and added together the Raman scattering irreducible tensor components.[20–22] As was reported in Paper I, the actual relative electronic Raman intensity calculation in DyAlG at $T>T_N$ was carried out by using the wave functions which resulted from our CF analysis. Since the Kramers degeneracy is not lifted at $T>T_N$ and $H_{app}=0$, the intensity contributions from each member of the Kramers doublet were added to give the total Raman scattered intensity.

In this work, we must deal with a different situation. At $T<T_N$ and $H_{app}=0$, the internal magnetic interactions among the Dy^{3+} ions lead to the (A_1, A_1, A_1) configuration. The ions at the six different sites experience the same internal magnetic field, which causes the splitting of the Kramers doublets. Thus, in deriving the Raman tensor, we can no longer simply add the contributions from each of the Kramers states for two reasons: First, for kT much less than the ground doublet splitting, only the lower ground doublet is populated; second, the transitions from the ground state to the excited doublets (lower and higher) have different energies. The resulting Raman scattering tensor is given in Table III(a), which is like Table V(a) in Paper I except that the contributions from each member of the Kramers doublet are not added. A given Raman peak then only involves a $\Delta J_z=\pm1$ transition or a $\Delta J_z=0,\ \pm2$ transition, but not both. Such transitions are shown in Fig. 4 as peaks I and I′.

When we apply a field along [001] and have the (P_d, P_d, P_m) configuration, the six Dy^{3+} ions no longer have the same energy structure. Two of the six sites have spins aligned along [001], and their Kramers doublets are split by an amount $\Delta=\mu_B g_z(H_{app}-NM+H_{internal})$. The Raman transitions involving these two ions result in two lines in the Raman spectra (assuming only the bottom level of the ground doublet is populated). Owing to the nature of the crystal-field wave functions, usually one of the peaks is stronger, involving the ground state and either the upper or lower of the excited-state doublets. The resulting Raman scattering tensor is given in Table III(b), and schematically shown in Figs. 3 and 4 as peak III.

The other four Dy^{3+} ions have spins aligned transverse to the field applied along [001]. Thus their Kramers doublets are split by an amount $\Delta=\mu_B[\frac{1}{2}(g_x^2+g_y^2)]^{1/2}\ (H_{app}-NM+H_{internal})$, which is much less than the splitting for the two Z-oriented spins. The splitting of the ground-state doublet with $H_{app}=18$ kOe is typically $\Delta\sim0.5$ cm^{-1}. Thus at $T=1.5$ K, both levels of the doublet are populated. Hence, in deriving the Raman tensor, both levels of the ground-state doublet contribute to each transition, and the two contributions are assumed in this paper to add equally as if they were degenerate (see peak II of Figs. 3 and 4). Since the doublet splittings of levels 1 and 2 are less

TABLE III. Relative electronic Raman intensities for all polarization combinations (see Fig. 1) in terms of the spherical scattering tensor components. (a), (b), and (c) are associated with peaks I, II, and III, respectively.

(a) (A_1, A_1, A_1) (peak I)

	$\Delta J_z = 0, \pm 2$	$\Delta J_z = \pm 1$
V-V	$2(\alpha_0^2)^2 + (\alpha_2^2 - \alpha_{-2}^2)^2$	0
H-H	$(\alpha_0^1)^2 + \frac{3}{2}(\alpha_0^2)^2 + \frac{3}{4}(\alpha_2^2 - \alpha_{-2}^2)^2$	$(\alpha_1^1)^2 + (\alpha_{-1}^1)^2$
H-V = V-H	$(\alpha_0^1)^2 + \frac{1}{2}(\alpha_2^2 + \alpha_{-2}^2)^2$	$(\alpha_1^1)^2 + (\alpha_{-1}^1)^2 + (\alpha_1^2)^2 + (\alpha_{-1}^2)^2$
	(upper or lower)	(lower or upper)

(b) Parallel: (P_d, P_d, P_m) (peak III)

	$\Delta J_z = 0, \pm 2$		$\Delta J_z = \pm 1$
V-V	$\frac{4}{3}(\alpha_0^2)^2$	+	0
H-H	$\frac{1}{2}(\alpha_2^2 - \alpha_{-2}^2)^2 + (\alpha_0^1)^2$	+	0
H-V	0	+	$\frac{1}{2}[(\alpha_1^2)^2 + (\alpha_{-1}^2)^2 + (\alpha_1^1)^2 + (\alpha_{-1}^1)^2] + [\alpha_1^2\alpha_1^1 - \alpha_{-1}^2\alpha_{-1}^1]$
V-H	0	+	$\frac{1}{2}[(\alpha_1^2)^2 + (\alpha_{-1}^2)^2 + (\alpha_1^1)^2 + (\alpha_{-1}^1)^2] - [\alpha_1^2\alpha_1^1 - \alpha_{-1}^2\alpha_{-1}^1]$

(c) Transverse: (P_d, P_d, P_m) (peak II)

	$\Delta J_z = 0, \pm 2$	$\Delta J_z = \pm 1$
V-V	$\frac{2}{3}(\alpha_0^2)^2 + (\alpha_2^2 - \alpha_{-2}^2)^2$	0
H-H	$\frac{3}{2}(\alpha_0^2)^2 + \frac{1}{4}(\alpha_2^2 - \alpha_{-2}^2)^2$	$(\alpha_1^1)^2 + (\alpha_{-1}^1)^2$
H-V	$(\alpha_0^1)^2 + \frac{1}{2}(\alpha_2^2 + \alpha_{-2}^2)^2$	$\frac{1}{2}[(\alpha_1^2)^2 + (\alpha_{-1}^2)^2 + (\alpha_1^1)^2 + (\alpha_{-1}^1)^2] - [\alpha_1^2\alpha_1^1 - \alpha_{-1}^2\alpha_{-1}^1]$
V-H	$(\alpha_0^1)^2 + \frac{1}{2}(\alpha_2^2 + \alpha_{-2}^2)^2$	$\frac{1}{2}[(\alpha_1^2)^2 + (\alpha_{-1}^2)^2 + (\alpha_1^1)^2 + (\alpha_{-1}^1)^2] + [\alpha_1^2\alpha_1^1 - \alpha_{-1}^2\alpha_{-1}^1]$
	(upper or lower)	(lower or upper)

than our experimental spectral resolution, the Raman scattering tensor is derived as if the lines are unsplit, and is given in Table III(c). Of course, the formulas of Tables III(b) and III(c) must add up to give that of Table III(a).

The relative electronic Raman intensities have been calculated for this present situation using the actual wave functions determined by the CF analysis of DyAlG at 80 K. The calculated relative intensities are only qualitatively like the experimental Raman spectra. One feature the calculations do predict is the reversal of intensities of peaks II and III upon changing the polarization combinations from H-V to V-H (see Fig. 6 for 0-0′ transition). This theoretical prediction for H-V and V-H can be readily seen by observing that in going from Table III(b) to Table III(c), the two lower right-hand expressions involved a change of sign between the two bracketed terms.

Two additional features are predicted by our calculations: First, for the 0-0′ transition, the Raman intensity of peak II should be twice as large as peak III for V-H polarizations. This was observed experimentally as exhibited in Fig. 6. Secondly, the intensities in V-H and H-V polarizations should be stronger than in H-H and V-V. The calculated and observed results for the H-H

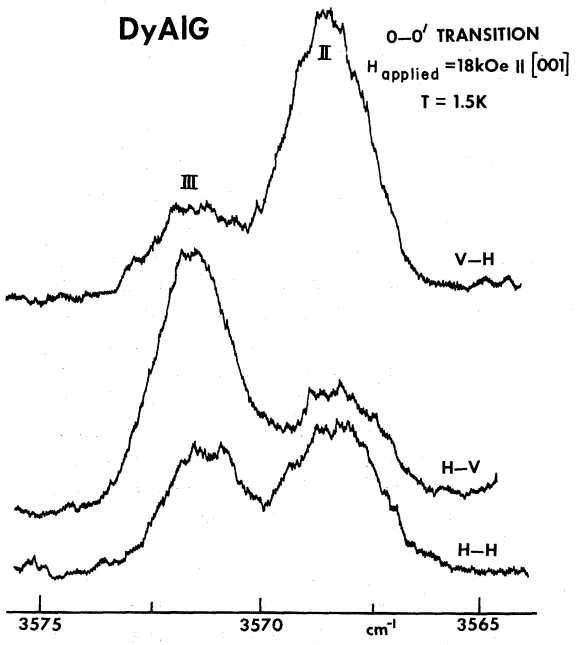

FIG. 6. Raman spectra, pertaining to 0-0′ electronic transitions, observed for different incident-scattered polarizations (V-H, H-V, and H-H). The reversal of intensities of peaks II and III upon changing the polarizations from H-V to V-H was predicted by theory. [See Tables III(b) and III(c).]

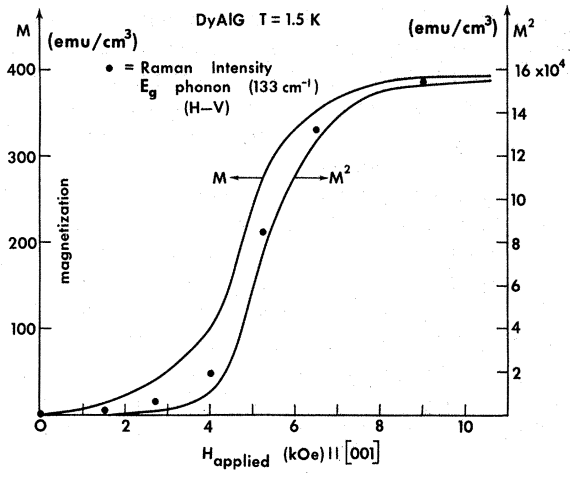

FIG. 7. Observed Raman intensity due to the E_g (133 cm^{-1}) phonon as a function of the applied magnetic field. For the H-V polarizations, Raman scattering from the E_g phonons is forbidden for crystals of O_h and C_{4h} point groups (see Table IV). The intensity at 9 kOe was normalized to 385 relative units (same scale as M). The magnetization and the square of the magnetization versus applied field data were obtained from Ref. 18 and are shown here for comparison purposes.

disagreed significantly. This may indicate that our estimates for the radial matrix elements $(4f|r^2|4f)$ and $(4f|r|5d)$,[20–22] and probably the wave functions as determined by the least-squares fit to the observed CF energy levels of Paper I, may not be sufficiently accurate to predict intensities for the electronic transitions.

VI. PHONONS

All the Raman-active phonons ($3A_{1g}+8E_g+14T_{2g}$), with the exception of one E_g phonon, have been recently reported by us in Paper I (see also Ref. 18). These phonons all obeyed polarization selection rules.[23] Using an optimum crystal orientation, the symmetry of the phonons was readily identified by the presence or absence of Raman scattering for a given combination of incident-scattered polarizations. The orientation of the crystal with respect to the incident and scattered propagation directions in this work (see Fig. 1) is identical to that used in Paper I. The results of the polarization selection rules are summarized in Table IV for DyAlG (O_h point group).

In the present experiment, for $T = 1.5$ K and $H_{app} = 0$ kOe, the polarization selection rules were examined for A_{1g}, E_g, and T_{2g} phonons and were found to be strictly obeyed (their wave numbers were all about $+2$ cm^{-1} higher than at 80 K). This result assured us that the crystal and the optical paths were oriented accurately.

Upon the application of a magnetic field along the [001] direction, the polarization selection rules for the E_g (130 cm^{-1}) and the A_{1g} (781 cm^{-1}) phonons were not obeyed. When H_{app} is increased from 0 to 10 kOe, the Raman intensity of E_g in the H-V polarization combination (forbidden) rises from zero to nearly the full Raman intensity observed in the H-H polarization combination (allowed). The increase in intensity versus applied field is shown in Fig. 7, where the magnetization as determined by Wyatt[19] and the square of the magnetization versus H_{app} are also shown. The "forbidden" E_g intensity appears to follow M^2 more closely than M. Assuming that the magnetostriction in DyAlG has lowered the initial O_h point-group symmetry to C_{4h}, the Raman scattering from the E_g phonons is still forbidden in the H-V and V-H polarization combinations (see Table IV). The behavior of the A_{1g} phonon (781 cm^{-1}) is similar.

Another possible explanation of the peculiar phonon intensities was that the DyAlG crystal rotated upon application of the external magnetic field. However, since the glass rod, the DyAlG crystal, and the prism (shown in Fig. 1), were held rigidly together by a brass sleeve, any slight rotation of the DyAlG would have resulted in a rotation of the prism. This would have markedly changed the transmitted pattern of the laser beam which was channeled through the glass light pipe. We observed no such change upon the application of the magnetic field. As a further confirmation that the DyAlG did not physically rotate for $H > 0$, we observed that the polarization selection rules for the T_{2g} phonons were still strictly obeyed for V-V and V-H. We are unable to propose a reasonable explanation as to why the polarization selection rules for all phonons are obeyed with $H_{app} = 0$, and why these rules are disobeyed for E_g and A_{1g}, but obeyed for T_{2g} phonons, with $H_{app} > 0$ along [001].

VII. CONCLUSION

Although the experimental results reported in this paper are preliminary, they do indicate the potential of electronic Raman spectroscopy in providing information on the effect of magnetic interactions on the rare-earth ions. Previously, we have reported in Paper I on the Raman-active phonons in DyAlG and the crystal-field levels be-

TABLE IV. Relative phonon Raman intensities for all polarization combinations (see Fig. 1) when the crystal has O_h or C_{4h} point-group symmetry.

	O_h Symmetry					C_{4h} Symmetry			
	V-V	V-H	H-V	H-H		V-V	V-H	H-V	H-H
A_{1g}	a_1^2	0	0	0	$\rightarrow A_g$	b^2	0	0	0
E_g	$\frac{4}{3}a_{12}^2$	0	0	a_{12}^2	$\rightarrow A_g+B_g$	b^2	0	0	c^2
T_{2g}	0	a_{25}^2	a_{25}^2	0	$\rightarrow B_g+E_g$	0	e^2+f^2	e^2+f^2	c^2

longing to the $^6H_{15/2}$ and $^6H_{13/2}$ manifolds, which, when supplemented by higher-manifold data, enabled us to perform a complete crystal-field analysis. In this paper, we used these crystal-field wave functions to calculate the g values of all the levels in the lower two manifolds. Wherever comparisons with existing experimental data were possible, our calculated g values were in good agreement.

We have observed in DyAlG at $T = 1.5$ K shifts and splittings in the Raman data upon application of an external magnetic field ($H_{app} = 18$ kOe) parallel to [001] as compared to the spectra with $H_{app} = 0$ kOe. Using the information existing in the literature on the ground-state splitting of DyAlG for $T = 1.5$ K and $H_{app} = 0$ kOe, we were able to deduce the following data for the first two excited levels in the $^6H_{15/2}$ manifold: (i) the exchange fields when the spin configuration is (A_1, A_1, A_1), and (ii) the exchange fields when the spin configuration is (P_d, P_d, P_m). The g_z value of the lowest level in the $^6H_{13/2}$ manifold has been measured ($g_z = 14.7 \pm 1.0$) and was found comparable to our calculated value, $g_z = 15.0$.

The electronic Raman scattering tensors appropriate to the (A_1, A_1, A_1) and (P_d, P_d, P_m) spin configurations were derived in this paper. The relative Raman intensities were calculated using CF wave functions obtained from our previous CF analysis. Only fair qualitative agreement between the calculated and observed electronic Raman peaks was found. Further work is required to achieve better correlation between the calculated and experimental Raman intensities for the four combinations of incident and scattered polarizations. The calculated intensity results were, however, helpful in assigning the lines in the observed spectra to specific electronic transitions. Peculiarities observed in the polarization selection rules for the A_{1g} and E_g but not for the T_{2g} Raman-active phonons when $H_{app} = 18$ kOe and $T = 1.5$ K are reported in this paper. No explanation can be given at this time.

ACKNOWLEDGMENTS

We particularly wish to thank Professor W. P. Wolf of Yale University for several most helpful discussions regarding the magnetic interactions in DyAlG and for making the theses of his former students available to us. The DyAlG crystal of excellent optical quality was flux grown by Stanley Mroczkowski, and we wish to express our sincere appreciation to him.

---

*Work supported in part by the Air Force Office of Scientific Research under Grant No. F44620-69-C-0102 and the National Science Foundation under Grant No. GK-12509.

†Present address: IBM Thomas J. Watson Research Center, Yorktown Heights, N. Y. 10598.

‡Present address: Bell Telephone Laboratories, Murray Hill, N. J. 07974.

[1]K. H. Hellwege, S. Hüfner, M. Schinkmann, and H. Schmidt, Phys. Letters 12, 107 (1964).

[2]A. H. Cooke, K. A. Gehring, M. J. M. Leask, D. Smith, and J. H. M. Thornley, Phys. Rev. Letters 14, 685 (1965).

[3]K. Aoyagi, K. Tsushima, and M. Uesugi, J. Phys. Soc. Japan 27, 49 (1969).

[4]K. A. Gehring, M. J. M. Leask, and J. H. M. Thornley, J. Phys. C 2, 484 (1969).

[5]R. Faulhaber and S. Hüfner, Z. Physik 228, 235 (1969).

[6]D. P. Landau, B. E. Keen, B. Schneider, and W. P. Wolf, Phys. Rev. B 3, 2310 (1971).

[7]M. Ball, M. T. Hutchings, M. J. M. Leask, and W. P. Wolf, in *Proceedings of the Eighth International Conference on Low Temperature Physics* (Butterworth, London, 1963), p. 248.

[8]W. P. Wolf, B. E. Keen, D. P. Landau, and B. Schneider, in *Proceedings of the Tenth International Conference on Low Temperature Physics, Moscow*, 1966, edited by M. P. Malkov (Vimitti, Moscow, U.S.S.R., 1967), Vol. IV, p. 136; Fig. 2 summarizes the configurations of spin alignment.

[9]P. M. Levy, Phys. Rev. 177, 509 (1969).

[10]W. P. Wolf, J. Phys. (Paris) Suppl. 32, C1-26 (1971).

[11]R. L. Wadsack, Joan L. Lewis, B. E. Argyle, and R. K. Chang, Phys. Rev. B 3, 4342 (1971), referred to as Paper I in text. References to earlier works on phonon and electronic Raman scatterings in DyAlG at $T > T_N$ can be found in this paper.

[12]P. Grünberg, S. Hüfner, E. Orlich, and J. Schmitt, Phys. Rev. 184, 285 (1969).

[13]M. Ball, W. P. Wolf, and A. F. G. Wyatt, Phys. Letters 10, 7 (1964).

[14]M. Ball, M. J. M. Leask, W. P. Wolf, and A. F. G. Wyatt, J. Appl. Phys. 34, 1104 (1963).

[15]B. E. Keen, D. P. Landau, and W. P. Wolf, Phys. Letters 23, 202 (1966).

[16]B. Schneider, D. P. Landau, B. E. Keen, and W. P. Wolf, Phys. Letters 23, 210 (1966).

[17]D. P. Landau, thesis (Yale University, 1967), p. 7.10 (unpublished). Calculation was made only when H_{app} was along [111] resulting in a (P_m, P_m, P_m) configuration. The dipolar field was calculated to be 453 ± 10 Oe, while the measured internal field was 61 ± 115 Oe. In the present (P_d, P_d, P_m) configuration, the internal fields will still be small (private communication with D. P. Landau).

[18]G. Mace, G. Schaack, Toaning Ng, and J. A. Koningstein, Z. Physik 230, 391 (1970).

[19]A. F. G. Wyatt, thesis (Oxford University, 1963) (unpublished).

[20]J. D. Axe, Jr., Phys. Rev. 136, A42 (1964).

[21]J. A. Koningstein and O. Sonnich Mortensen, Phys. Rev. 168, 75 (1968).

[22]O. Sonnich Mortensen and J. A. Koningstein, J. Chem. Phys. 48, 3971 (1968).

[23]R. Loudon, Advan. Phys. 13, 423 (1964).